Oil & Natural Gas Technology

Final Report

Characterization and Decomposition Kinetic Studies of Methane Hydrate In Host Sediments Under Subsurface-mimic Conditions

Submitted by:
Energy Sciences & Technology Department
Brookhaven National Laboratory
Upton, NY 11973

Office of Fossil Energy

Project Summary Page

Characterization and Decomposition Kinetic Studies of Methane Hydrate In Host Sediments Under Subsurface-mimic Conditions

Cooperative Agreement No.:	DE-AC02-98CH10886
	FWP EST-380-NEDA
Contractor Names:	Brookhaven National Laboratory, Upton, NY
DOE Award:	$ 20,000
Principal Investigator:	Devinder Mahajan
Project Manager:	Richard Baker- National Energy Technology Laboratory
Type of Report:	Technical Report
Reporting Period:	June 2008 to December 2010

DISCLAIMER

Technical Summary

This report describes work that was completed at Brookhaven National Laboratory (BNL) between June 1, 2008 through December 31, 2009. The research focus of this effort was as follows: 1) Complete methane hydrate formation/ decomposition kinetics in consolidated cores and 2) Develop the computed tomography (CT) technique at the microscale for applicability to methane hydrate studies. First, the cell design, construction and its adaptability to the Beamline X-2B at the National Synchrotron Light Source (NSLS), BNL was successfully completed. Second, *in situ* formation of Tetrahydrofuran (THF)-hydrates (sII) and Methane hydrates (sI) hosted in uniform glass beads was demonstrated. The results from the THF-hydrate study are already published and presented at various meetings. The Methane-hydrate data are in preparation for submission to a refereed journal.

Complementing the research effort was the education and training effort. A Ph.D. student who worked on this project is defending his Ph.D. thesis in March 2010 at Stony Brook University. An undergraduate student, who worked on the project for the last two years, plans to continue her graduate work in the area of methane hydrate.

Three micro cells for systematically conducting computed microtomography (CMT) studies of methane hydrates in porous media are now available. The micro cells are also suited to studying the dynamics of the CO_2-CH_4 exchange, a reaction of interest to both the hydrate and the carbon sequestration communities. A proposal entitled, "*Imaging Methane Hydrate Growth in Porous Media at Microscale Using Computed Tomography: Potential Implication in Climate Change*" was submitted to DOE for consideration. Should funding for FY 2010 be made available, the effort will exclusively focus on continuing the CMT studies.

Table of Contents

List of Tables

List of Figures

Project Highlights

Runs in the FISH Unit

    The formation/decomposition kinetic study of consolidated cores continued during this reporting period. The TEMCO's DCHR-series hassler-type core holder was utilized to mimic natural temperature/pressure conditions below the seafloor. A total of 19 runs were completed in pure water and seawater hosted in Ottawa sand. The decomposition data were fitted in a model developed by Liang et al (2005) and the dissociation constants were extracted from these plots. One such value was 1.16×10^{-3} mol / MPa.sec.gm.

CMT Runs

    The development of the CMT technique was the main focus of this effort.

- The beamline X2B at,NSLS / BNL was used to discern the structural features of hydrates. The available fixed-beam energy at the beamline is limited to below 30 keV.

- Three micro cells of diameters 1", ½", ¼" were configured to conduct CMT imaging studies of methane hydrates. The total cell volume varied from 60 mL for the 1" cell to ~3 mL for the ¼" cell. The ¼" diameter cell fitted well in the x-ray beamline cell holder. Therefore, it was selected for the *in situ* runs.

- A series of experiments involving methane hydrate formation were conducted in the ¼" diameter cell to establish the effect of cell orientation on the extent of methane hydrate formation. A maximum of ~14% hydrate saturation was observed under certain conditions. The available x-ray resolution dictated that at least 5% methane hydrate saturation was needed to establish hydrate visualization with certainty.

- The THF-hydrate (sII) was used as a surrogate for CH_4-hydrate (sI). The THF-hydrate was formed from a 60 wt% THF-40 wt% H_2O-$BaCl_2$ /glass bead mixture in a 1 mL polypropylene syringe-cell. The time resolved data were reconstructed in 2-D and 3-D images to show that the

formed hydrates grew in pores in a manner similar to known pore-filling models. The hydrates were patchy and appeared to displace glass beads during the process.

- The CH_4-hydrates were formed from a CH_4/H_2O-$BaCl_2$ /glass bead mixture in the ¼'' diameter cell at 966 psig at -1.4 °C. The time resolved data were reconstructed in 2-D and 3-D images to show that the formed hydrates grew in pores in a manner similar to those observed for the THF-hydrate system. The hydrates were patchy and appeared to displace glass beads during the process.

Technical Work Description

Below we describe the tasks that were either completed or initiated during this reporting period.

1. Runs in the FISH Unit

1-1. Methane hydrate formation/decomposition runs

The formation/decomposition kinetic study of consolidated cores continued during this reporting period. The TEMCO's DCHR-series hassler-type core holder was utilized to mimic natural geothermal conditions below the seafloor. The core sample (2"diameter and 0-6" length) was held within a rubber sleeve by radial confining pressure. The fluids and gases were injected through distribution plugs. The unique arrangement of ports along the length of the core enabled to draw a radial and axial temperature profile within the core during hydrate formation/dissociation. The effect of varying the overburden pressure (confining pressure) and temperature was studied.

In a typical hydrate formation/dissociation run, methane gas (purity: 99.99%) was charged at a controlled flow rate (< 2000 mL/min) through a 0.6μm average pore diameter CoorsTek porous ceramic filter (2" diameter, 0.25" thickness) placed above and below the core. Three type J (1/16" diameter) thermocouples were installed at 1", 3", and 5" along the core length. Ottawa sand, from the US Silica Company, served as hosts.

A set of run conditions for the Ottawa sand as host is given in Table 1. The experimental conditions for already completed and reported runs (1-7) are listed in Table 2. The hydrate formation methodology used is as follows. With 1300-1500 psig confining pressure and Ottawa sand-pack maintained at a set temperature with the bath cooled using ethylene glycol, methane gas was charged up to the desired pressure at flow rates of <2000 mL/min. After charging, hydrate formation P/T kinetics was monitored with time until pore pressure asymptoted at the hydrate equilibrium pressure.

The next set of runs (Runs 8-13, Table 3) was also performed but using a different methodology for hydrate formation. The hydrate formation in these runs was achieved by single gradual charging of methane through the completely water saturated sand-pack under confining pressure, up to the desired pressure and then cooling the cell down to the desired temperature.

The third set of runs (Runs 14-19, Table 4) utilized seawater and hydrates were formed under conditions similar to those listed for runs in Table 3.

For all completed runs, gas consumption during formation and gas evolution during decomposition data were collected. A typical run data for these events are shown for Run 9. Upon cooling, the system ultimately attained the P-T conditions (1220 psig, 11.4^{o}C) and then the methane hydrate stability region after 7.8 hours (Figure 1a). However, the hydrate formation began at ~13.8 hours i.e. 6 hours after the system entered the hydrate stability region. The sudden pressure drop and the exothermic peaks due to hydrate formation are shown in Figure 1b. The system followed pure water-methane stability curve established with CSMGem (Figure 2). The temperatures at the outer core surface (T1), half-way radius (T2), and the center of the core (T3) indicate that hydrates may have begun to form around the center and half-way radius of the core.

The dissociation was achieved by step-wise depressurization of the system. The entire dissociation event for Run 9 is shown in Figure 3a. The dissociation at each depressurization step was quick. As gas was released due to depressurization, the sediment temperature dropped due to endothermic hydrate dissociation and gas expansion. It is evident that the greater the pressure drops during dissociation, higher the degree of cooling and longer time period were observed for sediments to reach the initial *in-situ* temperature. The highest pressure drop of 115 psi during dissociation of Run 9 resulted in the sediment cooling of as low as 1.8^{o}C. As the gas output ceased, the cell exit valve was closed after which the sediment temperature was allowed to equilibrate with the bath temperature. This allowed all dissociation data at a constant temperature- the bath temperature. Figure 3b shows post-dissociation pressure-temperature equilibrium during sediment warm-up to the bath temperature. The post-depressurization dissociation was thermally induced where the system followed the hydrate PT equilibrium. However, this effect was seen until the hydrates were present within the sediments. After the

sixth pressure drop (dp6) of 89.2 psi, the hydrate dissociation was complete and subsequent post-dissociation curves represent methane gas warm-up. The post-dissociation responses for hydrates are slightly shifted towards higher pressure from the theoretical pure methane hydrate P-T stability curve (Figure 1b). This is due to the minimal excess pore (48.3 - 58.7 µm) pressure generated during subsequent thermally induced dissociations. The thermocouple responses also indicate that the core boundary experiences lesser degree of cooling during depressurization than half-radius and the center of the core. This implies that the hydrates may have been predominantly formed within the interior part of the core. However during thermally induced dissociation, the core boundary warms up at a faster rate as expected than the core half-radius and the core center. These data are summarized in Figure 3.

1-2. Modeling decomposition kinetic behavior of hydrate dissociation

Liang et al. (2005) studied the decomposition behavior of methane hydrates formed in porous activated carbon (5 mL) host from pure free water and methane in the presence of a surfactant (an aqueous solution of sodium dodecyl sulfate (SDS) of concentration 650 gm/m^3). The authors then fitted the decomposition rate data in a model developed for decomposition kinetic behavior of methane hydrates. The model is based on the ice-shielding mechanism in which a porous ice layer is assumed formed during the decomposition process. The model assumes the following two steps, of which the latter is assumed to be controlling during dissociation.

1. Destruction of clathrates host lattice at the surface of hydrate particle and desorption of methane molecule from the surface of hydrate particle.
2. Diffusion of CH_4 through the ice layer

$$\frac{dn}{dt} = \left[\frac{1}{\frac{1}{k} + \frac{n^b}{D_s}} \right] (f_e - f_g) \tag{1}$$

where, n – cumulative moles of methane released at time t, moles

k – hydrate dissociation constant, mol./(MPa.sec.gm)

b – empirical constant, unitless

Ds – empirical constant, mol(b+1)/(m.MPa.gm.sec)

After integrating above equation with limits, t = 0, n = 0 and t = t, n = n,

$$t = \frac{n}{k.(f_e - f_g)} + \frac{1}{(f_e - f_g).D_s(b+1)}.n^{(b+1)} \tag{2}$$

Combining unknowns and re-writing yields,

$$t = \frac{1}{(f_e - f_g)}\left[\frac{n}{K_1} + \frac{1}{D_s.K_3}.n^{K_3}\right] \tag{3}$$

where unknowns are

K_1 = k, hydrate dissociation constant, mol./(MPa.sec.gm)

K_3 = b+1

Ds = empirical constant, mol(b+1)/(m.MPa.gm.sec)

We used this model to fit the decomposition data summarized in Figure 3. The number of moles of methane evolved for each pressure drop during depressurization are plotted against time (red curve in Figure 4) to yield k, the hydrate dissociation constant. Equation 3 was then used to generate a theoretical plot as follows. The pressure drop of 115 psi resulted into changing cell pressure from equilibrium value, Pe = 555 psig to Pg = 446 psig at a bath temperature of 4.1°C. The pressure values of Pe and Pg were converted into fugacity values viz: fe = 522.5 psi and fg = 429.5 psi, respectively using the Redlich-Kwong-Soave equation of state. The experimental data of time (t,sec), cumulative number of moles of methane produced (n) and the fugacity difference (Δf) of 93 psi (0.641 MPa) were iteratively fitted to yield the theoretical curve in Figure 4 (blue curve). The computed hydrate dissociation constant (k) was 1.16 x 10^{-3} mol./(MPa.sec.gm). This hydrate dissociation constant value is about 10,000 times smaller than that observed for the pure water system by Liang et al. (2005).

Similar analysis is being carried out to generate dissociation constants for all 19 runs listed in Tables 2, 3 and 4. These dissociation data will be useful to compare differences between pure water and seawater systems in which consolidated cores were formed.

2. Microstructure Investigation of Hydrates in Host Sediments

The *in situ* methane hydrate formation/decomposition studies were conducted at the beamline X-2B at NSLS, BNL. Universally, the available intensities of x-rays at beamlines at the light sources limit spatial volumes of the cells that must fit in a small cell holder for x-ray exposure. Our effort focused on the design and construction of a high-pressure cell that could utilize maximum cell volume and form at least ~5% methane hydrate to allow imaging by x-rays. The progress made in this area is discussed below.

2-1. High-pressure cell design and construction

Since methane hydrate formation requires high pressures, the construction of a cell of sufficient volume is a challenge. We considered several materials for construction. The grade 2 Ti was chosen since it has one of the lowest mass attenuation coefficients (Figure 5).

The specifications of Cell I are as follows: length: 21.5 cm; O.D.: 1/4"; Ti tube of wall thickness: 0.035" (rated at 4500 psig @ 70°F); volume: ~3.5 mL. The top end is connected to a SS quick-connect for loading the sample. The assembly is fitted with a pressure transducer (Omega PX4100) and a 1/16" type-K thermocouple to continuously monitor P/T conditions. A 3-way safety pressure relief valve is added to allow pressure release from the system at any time during the experiment. It is surrounded with clear vinyl tubing as the cooling jacket for continuous cooling to achieve low temperatures that facilitate methane hydrate formation (Figure 6).

Two more assemblies were constructed. These assemblies have the tube height at ~10 cm and they do not have individual cooling jackets. The tubes are inserted in a glycol/water bath to form methane hydrates.

2-2. Effect of cell orientation on the extent of methane hydrate formation

Our initial efforts to form methane hydrates at beamline X-2B were unsuccessful. Maximizing methane hydrate formation in small volumes of the cell is a challenge because low solubility of methane in water. Gas diffusion to the dissolved phase dominates that limits the extent of methane hydrate formation during the CMT measurements. Note that at least 5% hydrates must be formed to ascertain that the CMT data differentiates between hydrates and liquid water. We, therefore, conducted a series of experiments to establish the extent of methane hydrate formation from the $CH_4/H_2O/BaCl_2$ (5 wt%) solution system. The cooling bath temperature was set between $+2^o$ and -5^oC. The extent of methane hydrate formation was calculated from the decrease in the cell pressure. The noteworthy observations from the data in Table 5 are:

- The maximum pressure drop (hence methane hydrate formation) show that hydrates form in most cases.
- The maximum hydrate (13.7%) was measured in the horizontal (as opposed to vertical) cell orientation.

We, therefore, devised a procedure to form methane hydrate in the horizontal cell position and then conducted measurements by CMT (see below).

2-3. Data collection procedure and data reconstruction for visualization

During CMT runs, the images were recorded using a charge coupled device (CCD) camera (pixel size = 0.00393 mm, area = 1340 x 1035 pixels) with 3500-5000 ms exposure in a 0.15^o angular increment from angle 0 to 180° at the 24-26 keV X-ray beam line at NSLS, BNL. The particle size distribution of natural sediments typically span a broad range, however a uniform packing of 500 μm-sized glass beads was used to remove the uncertainty related to this heterogeneity. A 25 wt% $BaCl_2$ solution was used to enhance the density contrast between aqueous THF and THF-hydrate; it also lowered the freezing point of the $BaCl_2$/Water solution to -6.85^oC. To initiate THF-hydrate formation, the solution was cooled with a circulating fluid at $-3°C$, above the freezing point of solution. Hydrate formation was monitored over 79 hours by scanning 10 tomograms. Of the 10, three were selected with reconstruction for 300 vertical pixels from each tomogram file and then converting them into a stack of jpegs using IDL

tomography software. The conversion of each stack of images in to 3-D volume involved Cmtvis (Tomov and McGuigan, 2004) or ImageJ (Rasband, 2005) and volume rendering software, Drishti (Limaye, 2006). The final processing yielded contrasting images in which THF-Water, THF-hydrate, and glass beads could be differentiated based on their attenuation coefficients.

2-4. *In Situ* CMT Runs

2-4-1. Ambient pressure system- THF-hydrate formation hosted in glass beads

THF-hydrate is a convenient surrogate for methane hydrate because the former requires an ambient pressure to form. We selected THF-hydrate formation conditions from the phase diagram (Figure 7). For this study, a 60 wt% THF- 40 wt% H_2O-$BaCl_2$/glass bead mixture of total volume ~1 mm^3 was used as a sample in a 1 mL polypropylene syringe-cell fitted within a cooling jacket. The CMT data, after reconstruction using the procedure in Section 2-3, yield both 2-D and 3-D images (Figures 8 and 9).

The hydrate formation appeared to start at a few locations in the system before the first images were taken at 28 hours. Figure 8 shows the growth pattern of THF hydrate and its interaction with glass beads. Time lapse bead-to-bead matching indicates that the growth of hydrates displaces beads within the unconsolidated pack. Further, the 2-D images show that the hydrate size and shape is independent of container-walls. These observations are consistent with previous NMR data (Mork, 2000) and visual observations (Tohidi et al., 2001) that imply random nature of the nucleation process.

A magnified image of one of the growing hydrates from Figure 8 is shown in Figure 9. Clearly, the hydrates grow in pores in a manner similar to the pore-filling model described by Dvorkin et al (1999). This implies progressive but significant reduction of mechanical strength of the sediment upon dissociation of hydrates by retraction from the pore walls followed by their shrinkage in the pore space (Kleinberg et al., 2003). The hydrate dissociation in large pores may trap gas within pores until hydrate saturation reaches low values, permitting the flow of gas. Away from grain surfaces, the hydrate surface is convex (Fig. 9) indicating that THF, not hydrate, is the wetting phase – presumably in the form of a thin film. This is analogous to ice growth in porous media in which a water film remains unfrozen (Kleinberg and Griffin, 2005; Anderson

and Tice, 1971) and consistent with the contact angle arguments of Miller (1980) and Clennell (1999). The hydrate distribution is patchy even though the THF/H_2O/glass bead system is homogeneous. Note that the 60% THF: 40wt % H_2O solution used leaves excess THF.

Our experiments involve THF hydrate growing from excess THF in a 500 µm uniform glass bead pack. If the same results extend to natural gas hydrate accumulations in the earth, the interpretation of seismic surveys and sonic well logs would need to be reconsidered.

2-4-2. High pressure system- Methane hydrate formation hosted in glass beads

In the present work, the high-pressure CMT cell (1/4" outside diameter, total volume ~3.5 mL), shown in Figure 6, was utilized to follow in situ methane hydrate formation. The cell was kept in horizontal orientation throughout the formation event to allow for greater mass transfer and to provide large gas-liquid (G-L) interface. After the cell was flushed with distilled water and compressed air, 3 gm (bulk volume ~2 mL) 500 μm (0.5 mm) uniform diameter glass beads were loaded into the cell. Subsequently, the cell was reoriented in the horizontal position in order to arrange the glass beads along the height of the cell. A 5wt% $BaCl_2$ solution (~1 mL) was added to the cell within glass beads arranged in the horizontal cell. A 5 wt% $BaCl_2$ solution (density 1.02 gm/cc) was used to enhance the contrast between any formed hydrates (density 0.92 gm/cc) and the aqueous solution. The cell was evacuated and methane was then slowly charged till the target system pressure (~966 psig) was achieved with the cell still horizontal. After the cell pressure equilibrated to the room temperature, the cell was transported to the beamline X2B. The cell was submerged horizontally into the ethylene glycol bath pre-chilled to -1^oC, just above the freezing point of the 5 wt% $BaCl_2$ solution (-1.4 °C). After about 3 hours, the cell pressure dropped and stabilized corresponding to about 13% conversion to methane hydrates. Subsequently, the coolant flow regulated by another refrigerated circulator was started through the cooling jacket to maintain the cell temperature at -1^oC. After the beamline parameters such as stage height, beam intensity, lens, focusing were adjusted, the cell was placed into the beam for tomographic run. Several tomograms were acquired with beam intensity of 27 - 29 keV and 1200 images (pixel size: 7.42 μm) each taken every 0.15^o during the rotation of sample through 0 - 180° and with 3.5 sec exposure. The reconstructions were performed for each tomogram with 400 vertical pixels to create a stack of 2-D cross-sectional images of the cell from which the 3-D

volume was rendered for a specific volume and fine tuned to create a specific phase based on a histogram.

Figure 11 shows one of the images from the stack of 2-D images created from different tomograms. It is evident that the glass beads and the interstitial aqueous solution are held together on one side of the cell through cementation due to hydrates and capillary forces. The hydrates nucleate randomly in pores formed by randomly packed host glass beads during the nucleation process and may or may not involve the cell wall. The bead-to-bead matching indicates slight movement of beads during hydrate growth.

Figure 12 shows an image of 2965 x 2756 x 2980 μm^3 volume dimension after about 15.25 hours of cooling. Based on the histogram, specific phases are selected such as those shown from the same volume. Clearly, methane hydrates grow from the direction of the G-L interface, filling pores of glass beads. The methane hydrate (Structure I) distribution can also be seen as patchy consistent with natural hydrate occurrence (Tserkovnyak and Johnson, 2002) and our previous observation of THF hydrates (Structure II) (Kerkar et al., 2009).

The patchy nucleation coupled with pore-filling growth of methane hydrates observed here could be extended to the natural methane hydrate systems. If the natural systems fit the same model, it would significantly change the hydrate saturations and relative permeabilities of the hydrate zones. The pore-filling model also supports recent field studies at the Keathley Canyon site, Gulf of Mexico where hydrates were found in nodular and vertical fracture filling form in the shallow shaly sediments (Cook et al., 2008; Kastner et al, 2008; Lee and Collett, 2008). Moreover, hydrate dissociation from pores suggests a reduction in the bulk modulus of the pore fluid than that for load bearing hydrates (Waite et al., 2004). This effect would enhance on the onset of dissociation of hydrates from the pore walls and could have radical impact on seafloor stability.

Future Direction

Preliminary runs to form methane-hydrate hosted in uniform glass beads in micro cells for the *in situ* CMT study at the beamline are promising. The study should be extended to:

1. A systematic time resolved study to form methane hydrates hosted in depleted sediments that once contained natural methane hydrates. Several of these sediment samples are available from sites such as the Gulf of Mexico (GoM), India and others

2. The micro cells are also suited to study the dynamics of the CO_2-CH_4 exchange, a reaction of interest to both the Hydrate and the Carbon Sequestration communities.

A proposal entitled, "*Imaging Methane Hydrate Growth in Porous Media at Microscale Using Computed Tomography: Potential Implication in Climate Change*" was submitted to DOE for consideration. Should the funding for FY 2010 is made available, the effort will exclusively focus on the above proposed CMT studies.

References

Anderson, D.M., Tice, A.R., Proc.-Soil Science Society Am., 35, 47–54 (1971).

Clennell, B., Hovland, M., Booth, J.S., Henry, P., Winters, W.J., J Geophysical Res., 104, B10, 22985-23003 (1999).

Cook, A.E., Goldberg, D., Kleinberg, R.L., Marine and Petroleum Geology, 25, 932-941 (2008).

Dvorkin, J., Prasad, M., Sakai, A., Lavoie, D., Geophys. Res. Lett., 26(12), 1781-1784 (1999).

Kastner, M., Claypool, G., Robertson, G., Marine and Petroleum Geology, 25, 860-872 (2008).

Kerkar, P., Jones, K.W., Kleinberg, R.L., Lindquist, W.B., Tomov, S., Feng, H., Mahajan, D., Applied Physics Letter, 95, 024102, August (2009).

Kleinberg, R.L., Flaum, C., Griffin, D.D., Brewer, P.G., Malby, G.E., Peltzer, E.T., Yesinowski, J.P., Journal of Geophysical Research 108(B10): 2508. doi:10.1029/2003JB002389 (2003).

Kleinberg, R.L., Griffin, D.D., Cold Regions Science and Technology, 42, 63-77 (2005).

Lee, M., Collett, T., Marine and Petroleum Geology, 25, 924-931 (2008).

Liang, M., Experimental and Modeling Study on Decomposition Kinetics of Methane Hydrates in Different Media, J. Phys. Chem. B, 109, 19034-19041, 2005

Limaye, A., Drishti – Volume Exploration and Presentation Tool, Poster Presentation, Vis 2006, Baltimore, USA (2006).

Miller, R.D., Freezing phenomena in soils, Introduction to Soil Physics edited by D. Hillel, 254-299, Academic, San Diego, California (1980).

Rasband, W.S., ImageJ, U. S. National Institutes of Health, Bethesda, Maryland, USA, http://rsb.info.nih.gov/ij/, 1997-2005.

Tserkovnyak, Y., Johnson, D.L., Geophysical Research Letters, 29 (7), 1108 (2002).

Tohidi, B., Anderson, R., Clennell, B., Burgass, R.W., Biderkab, A.B., Geology, 29, 9, 867-870 (2001).

Tomov, S., McGuigan, M., Interactive visualization of higher dimensional data in a multiview environment, arXiv:cs.GR/0405048 (2004). http://arxiv.org/PS_cache/cs/pdf/0405/0405048v1.pdf

Waite, W.F., Winters, W.J., Mason, D.H., American Mineralogists, 89, 1202-1207 (2004).

Yun, T.S.. Francisca, F.M., Santamarina, J.C., Ruppel, C., Geophysical Research Letters, 32, p. LI0609, doi:10.1029/2005GL022607 (2005).

Education and Training

One of the goals of the BNL effort is to educate and train the next-generation researchers in methane hydrate R&D. To this effect, BNL continued to train students at both the graduate and undergraduate levels. Notable output is:

- A Ph.D. student who worked on this project is defending his Ph.D. thesis in March 2010 at Stony Brook University.
- An undergraduate student, who worked on the project for the last two years, is graduating with a degree in Chemical and Molecular Engineering in May 2010. She is a U.S. citizen and plans to continue her graduate work in the area of methane hydrate.

Project Output

Posters

- P. B. Kerkar, K. Horvat, K. W. Jones, D. Mahajan. Understanding Laboratory-scale Methane Hydrate Dissociation in Porous Media: A Model for Marine Hydrate Occurrences 3rd Annual Advanced Energy Conference (AEC), Hauppauge, NY, November 18-19, 2009.

- K. Horvat, P. Kerkar, K.W. Jones, D. Mahajan Microscale Methane Hydrate Growth in Host Sediments. 3rd Annual Advanced Energy Conference (AEC), Hauppauge, NY, November 18-19, 2009.

- P. Kerkar, K. Horvat, K.W. Jones, and D. Mahajan. Understanding Laboratory-scale Methane Hydrate Dissociation in Porous Media: A Model for Marine Hydrate Occurrences, was presented at the AGU Fall Meeting, San Francisco, CA, USA. December 15-19, 2008.

Refereed Papers

- P. Kerkar, K.W. Jones, K. Horvat, R. Kleinberg, D. Mahajan. Imaging time-resolved methane hydrates growth in porous media using synchrotron X-ray computed microtomography. For Submission to Phys. Rev. Lett. (2010).

- P. Kerkar, KW. Jones, R. Kleinberg, W.B. Lindquist, S. Tomov, F. Huan and D. Mahajan. Direct observations of three dimensional growth of hydrates hosted in porous media. Appl. Phys. Lett. 95: 024102 (2009).

Table 1. TEMCO core holder and host Ottawa sand specifications

Core holder	Temco DCHR-2.0 w/ 3 temperature ports
Core holder volume	308.9 mL
Core diameter	2 inch
Core length	6 inch
Sediment	462.42 gm of Ottawa Sand F110 (average grain diameter – 110 μm)
Sediment density	1.625 gm/mL
Volume of two ceramic filters	24.3 mL
Volume of sand	284.6 mL
Water saturation	~ 100%
Top thermocouple (T1)	Core outer surface
Middle thermocouple (T2)	Half- way of radii of the core
Bottom thermocouple (T3)	Core center

Table 2. Summary of operating conditions of hydrate formation/dissociation runs with pure water and methane charging into a pre-cooled cell.

Run	Core conditions P psig	T °C	Overburden pressure psig	Methane flowrate mL/min	Formation event	Dissociation condition ΔP from Equilibrium P, psig
1	1200	4	1300	<1950	1	100-200
2	1200	4	1300	<2000	1	P_{eqm}
3	1200	4	1300	<1871	1	100-200
4	1200	4	1300	<1916	2	100
5	1200	4	1300	<1677	2	200
6	1200	2	1300	<1594	2	200
7	1200	2	1300	<1759	2	100

Table 3. Summary of operating conditions of hydrate formation/dissociation runs with pure water and methane charging followed by cooling.

Run #	Core conditions P, psig	T,°C	Overburden pressure psig	Methane flowrate mL/min	Dissociation conditions ΔP from Equilibrium P, psig
8	1214	4	1500	<2000	40, 107, 199, 304, 124, 155
9	1311	4	1500	<2000	115, 115, 111, 108, 105, 89, 102, 105, 105, 131
10	1362	4	1500	<2000	182, 159, 152, 139, 166, 147, 99
11	1200	4	1300	<700	85, 168, 277, 338, 132, 112
12	1200	5.5	1300	<2000	79, 171, 267, 329, 130, 138, 103
13	1200	3	1300	<2000	84, 174, 273, 326, 220

Table 4. Summary of operating conditions of hydrate formation/dissociation runs with seawater and methane charging followed by cooling.

Run #	Core conditions P, psig	T,°C	Overburden pressure psig	Methane flowrate mL/min	Dissociation conditions ΔP from Equilibrium P psig
14	1200	4	1500	<2000	77, 85, 91, 74, 75, 75, 75, 75, 75, 76, 75, 75, 79, 75, 75, 75, 110
15	1300	4	1500	<2000	100, 99, 146, 100, 100, 100, 99, 94, 104, 103, 100
16	1350	4	1500	<2000	88, 99, 99, 99, 99, 103, 101, 102, 102, 104, 109, 100, 100, 134
17	1300	2	1500	<2000	111, 96, 99, 100, 100, 101, 100, 100, 100, 101, 103, 103, 99, 100, 104, 125
18	1330	6	1500	<2000	82, 126, 95, 100, 103, 102, 110, 102, 104, 102, 102, 103, 103, 103, 101, 102, 101, 128
19	1330	8	1500	<2000	101, 101, 102, 102, 102, 102, 102, 105, 104, 102, 103, 110, 98, 131

Table 5. Summary of methane hydrate formation runs performed in assemblies with cells of various diameters.

| Cell OD	Orientation	V_{liquid} mL	V_{gas} mL	T_{bath} C	P_i at RT psig	P_i at T_{bath} psig	P_f psig	ΔP psig	Conversion %
1"	Vertical	20	39.85	-1	960.59	884.59	861.65	22.93	1.44
	Horizontal	20	39.85	-1	961.04	885.01	848.48	36.53	2.30
	Horizontal	10	49.85	-5	953.26	864.71	843.68	21.04	3.36
	Horizontal	10	49.85	-10	967.68	861.18	837.95	23.23	3.78
	Horizontal	10	49.85	-2.5	939.85	860.62	843.55	17.07	2.70
1/2"	Vertical	10	9.88	-1	983.37	909.43	924.31	0	0
	Vertical	10	9.88	-1	988.63	909.43	930.49	0	0
	Vertical	10	9.88	-5	986.34	900.87	903.14	0	0
	Vertical	10	9.88	-10	977.65	890.16	961.28	0	0
	Vertical	10	9.88	-2.5	969.18	906.22	912.87	0	0
	Horizontal	10	9.41	-1	950.98	889.25	855.07	34.18	1.01
	Horizontal	10	9.41	-1	958.76	889.25	827.94	61.30	1.82
	Horizontal	5	14.41	-1	960.71	889.25	846.94	42.31	3.85
1/4"	Horizontal	2	6.24	-1	951.31	919.07	875.62	43.44	4.28
	Horizontal	2	6.24	-1	954.89	919.07	861.38	57.69	5.68
	Horizontal	**1**	**7.24**	**-1**	**954.29**	**919.07**	**858.90**	**60.16**	**13.74**
	Horizontal	1	2.85	2	953.26	924.24	892.57	31.67	2.82
	Horizontal	1	2.85	2	956.09	924.24	889.71	34.52	3.07

(a) **(b)**
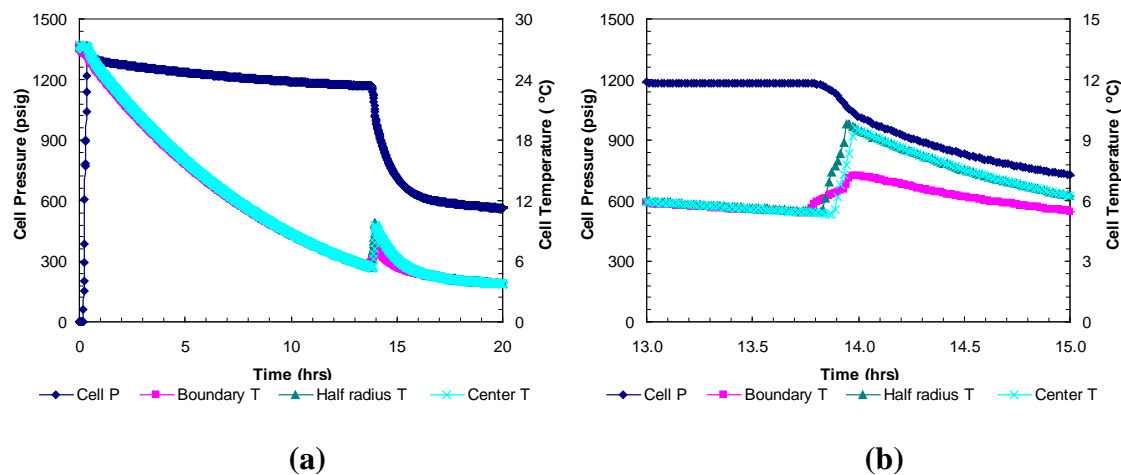
Figure 1. Core pressure/temperature versus time during (a) methane charging and subsequent hydrate formation for Run 9. A magnified view of the core conditions during hydrate formation event is shown in plot (b).
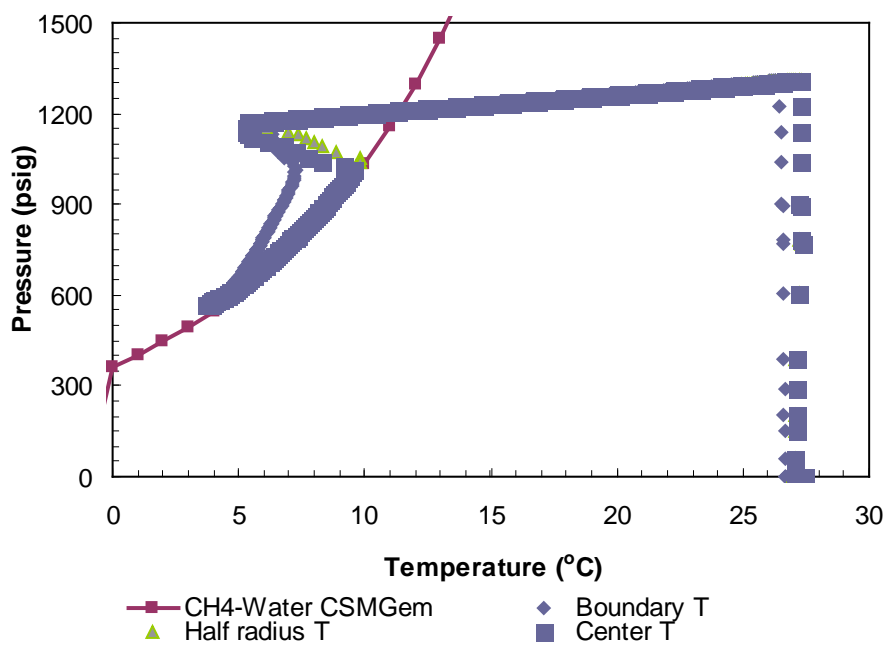

Figure 2. Comparison of core pressure/temperature during hydrate formation for Run 9 with a pure water-bulk methane hydrate stability curve obtained from CSMGem.
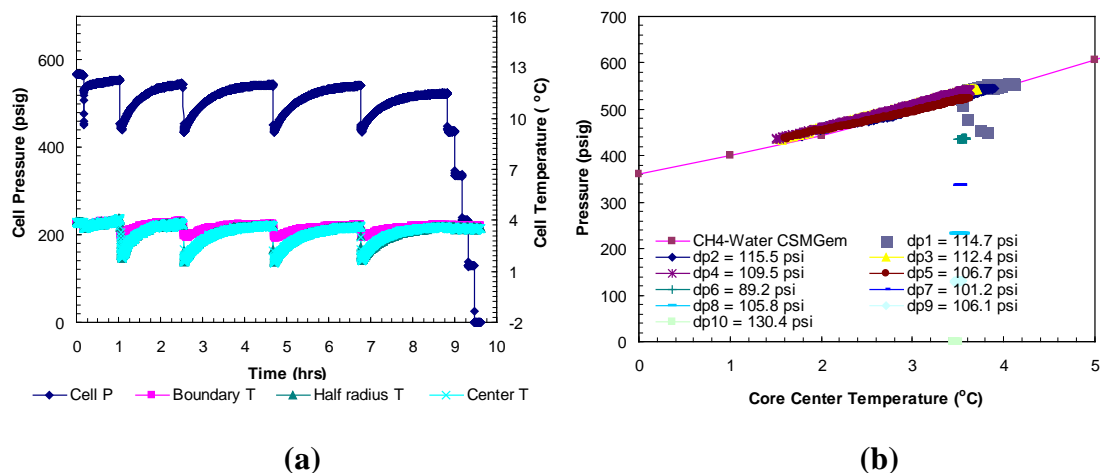
(a)   **(b)**

Figure 3. Core pressure/temperature versus time (a) during dissociation with varying pressure drops from equilibrium pressure in Run 9. Post-dissociation equilibrium pressure/temperature conditions of methane hydrates in porous media are shown in plot (b). Each plot corresponds to core conditions during thermally induced dissociations after each depressurization step. Equilibrium conditions of bulk methane hydrates were obtained from CSMGem.
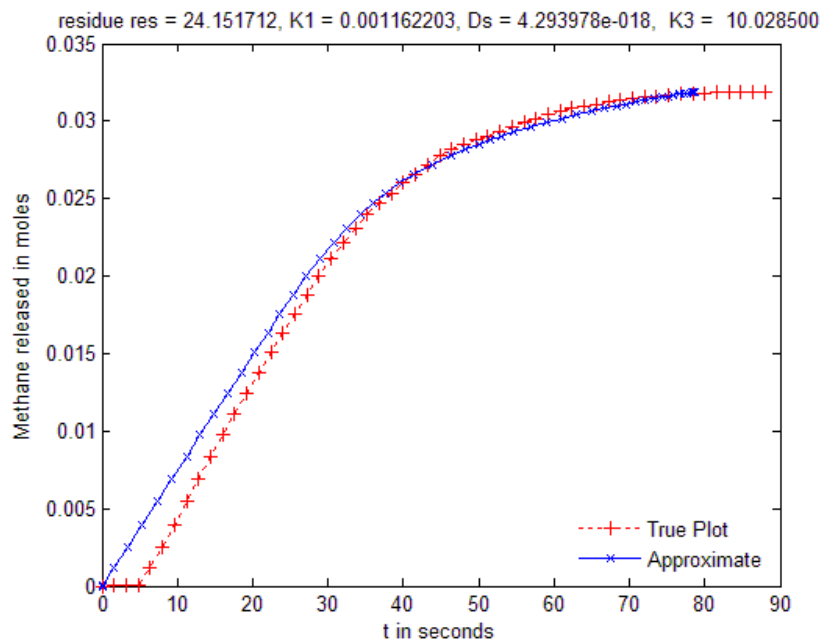
Figure 4. Experimental and model parameters curves for cumulative moles of methane evolved during dissociation due to a depressurization
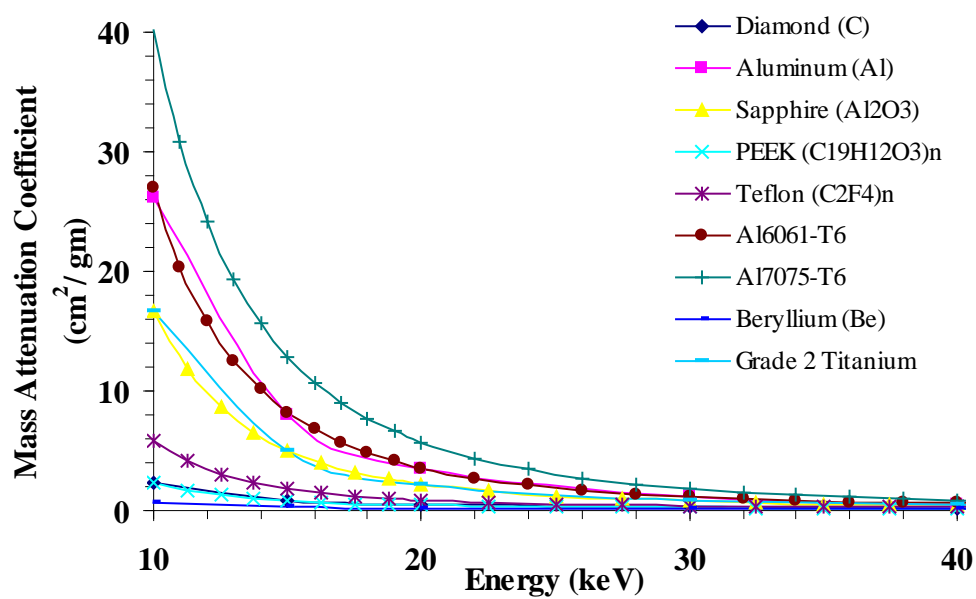
Figure 5. Mass Attenuation Coefficients of High Pressure Cell Materials
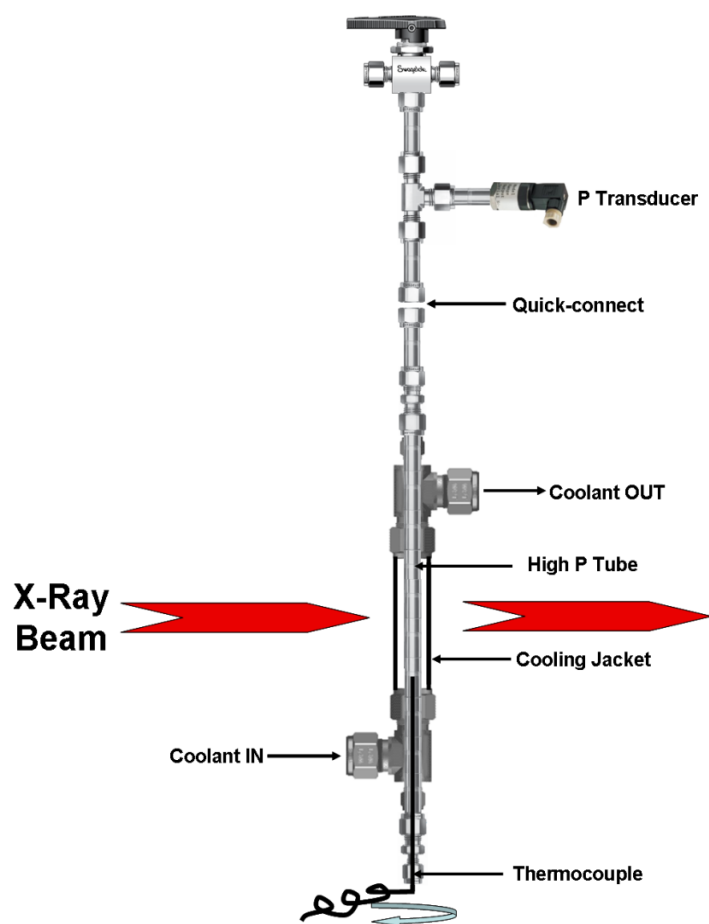
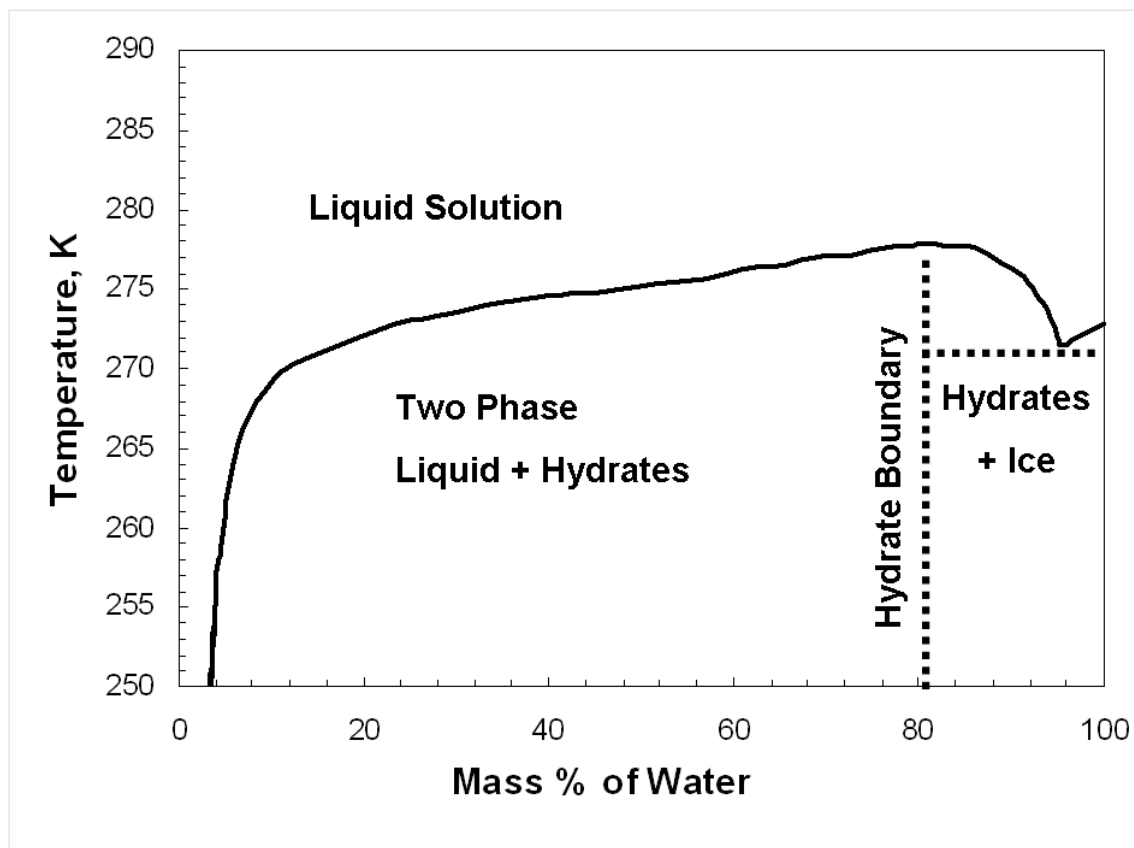Figure 6: Basic high-pressure CMT cell configuration for imaging methane hydrates.

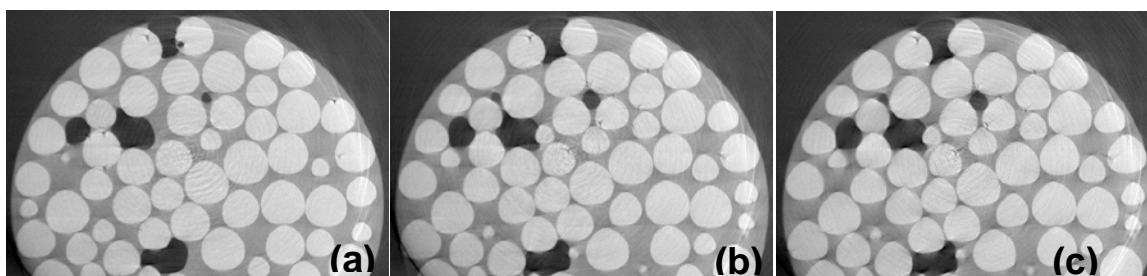Figure 7. THF-water phase diagram at 1 atmosphere (Yun et al., 2005).

Figure 8. Observation of random THF hydrate (black) growth hosted in glass beads (white spheres) is representative of 2-D cross sections (7 mm diameter). The images are recorded at (a) 54:06 h (b) 70:30 h (c) 74:07 h.
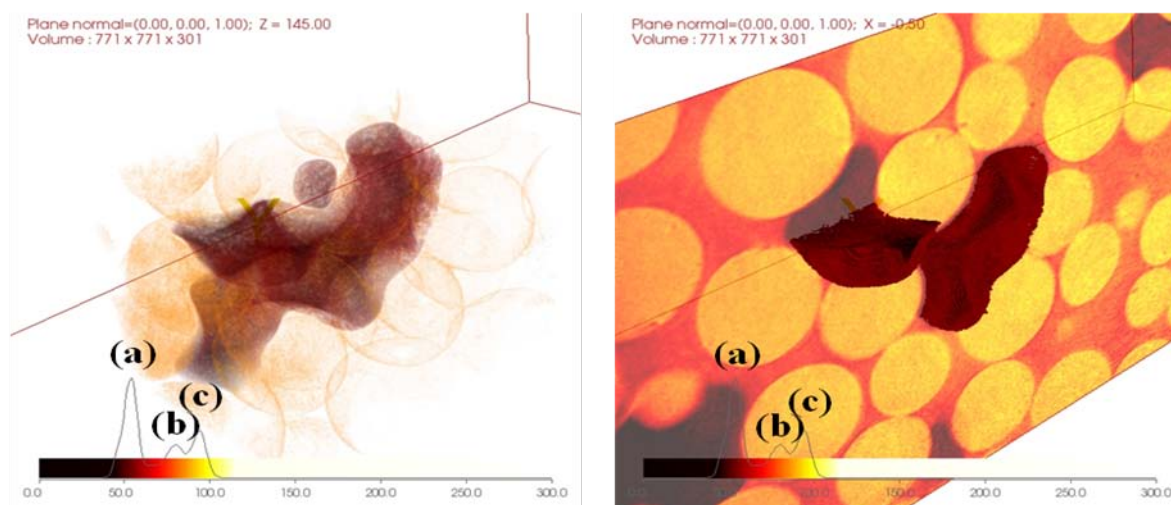

Figure 9. 3-D images of THF-hydrate in glass beads. The image was reconstructed from 300 slices such as those shown in Fig. 8. The embedded bar and accompanying graph relates to absorption coefficients that clearly differentiate hydrate (a), liquid THF and water (b), and glass beads seen as faded spheres (c).
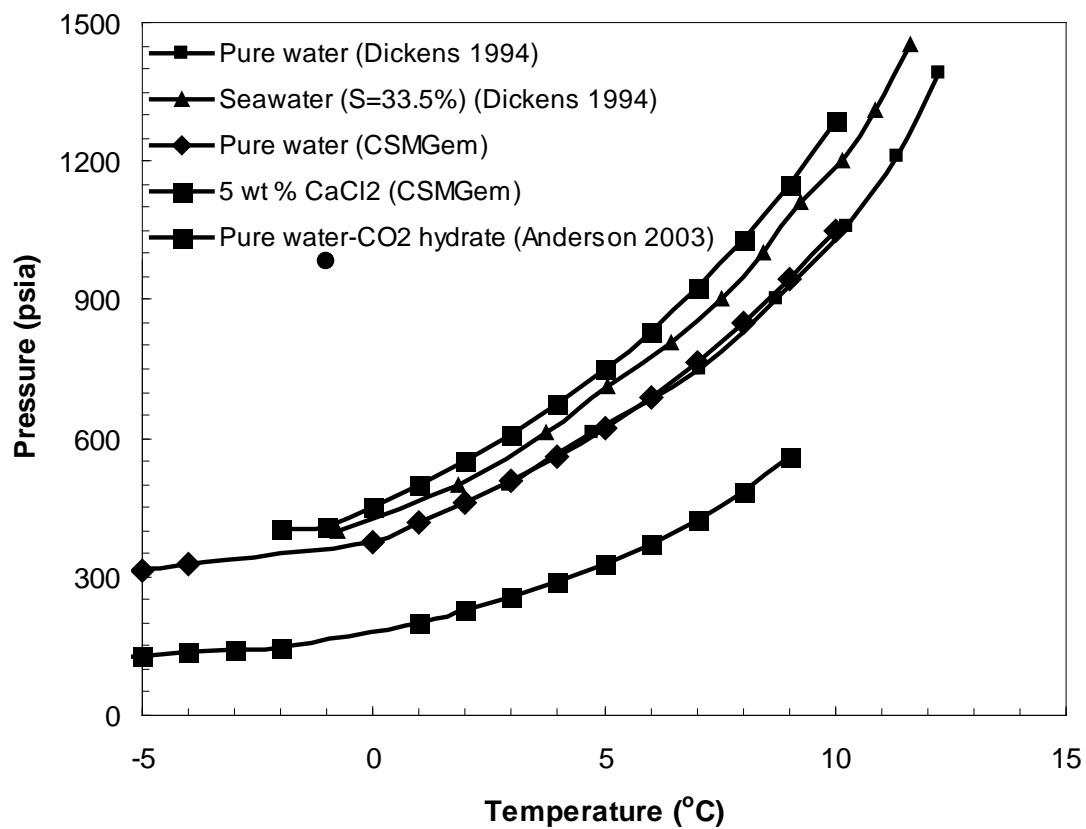
Figure 10. Pressure-temperature stability diagram for methane hydrates formed from pure and seawater and CO_2 hydrates formed from pure water.
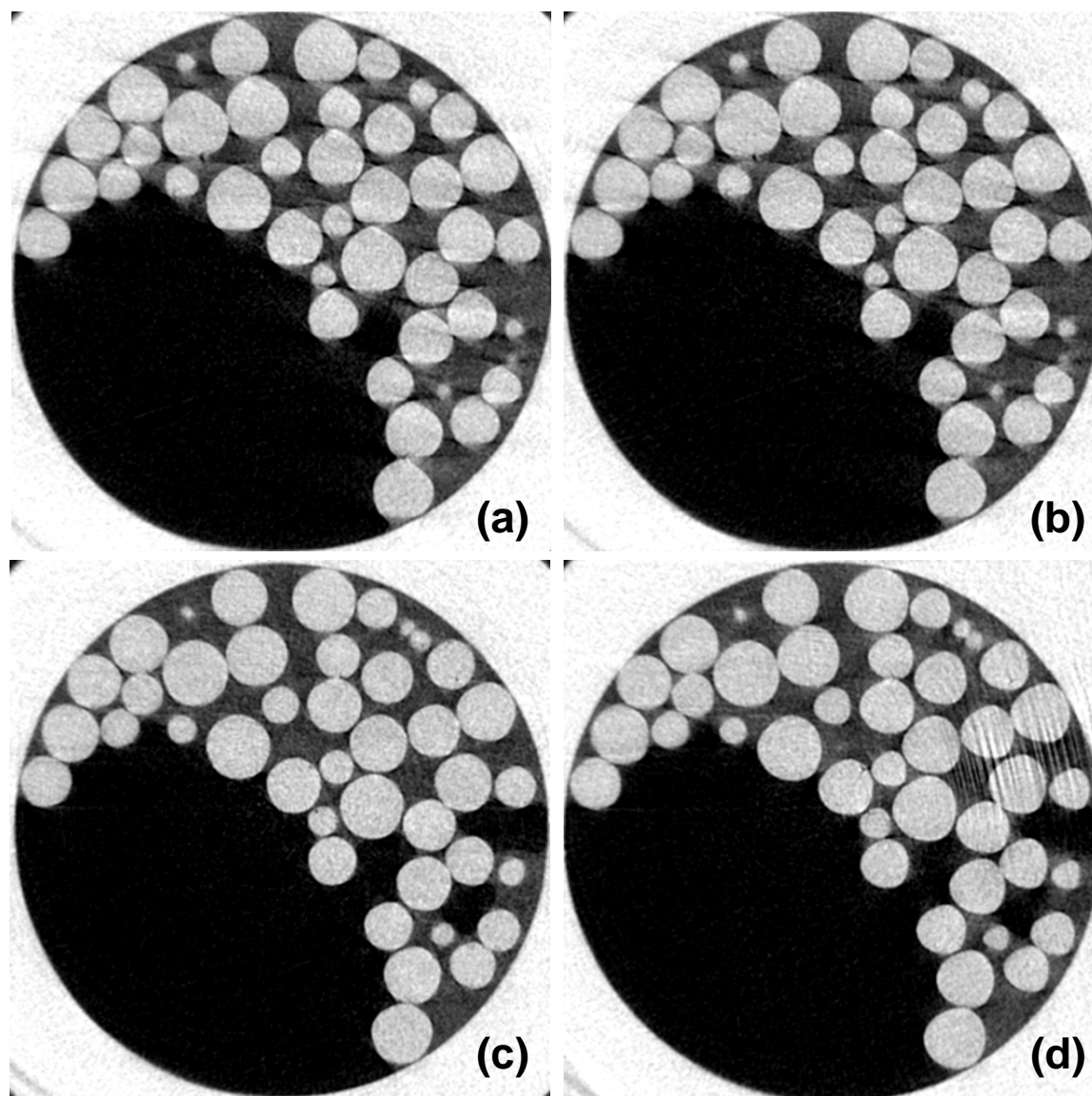
Figure 11. Observation of random methane hydrate growth hosted in glass beads (white spheres) is representative of 2-D cross sections (4.6 mm diameter). The images were recorded at (a) 15:15 h, (b) 19:19 h, (c) 24:54 h and (d) 49:14 h.
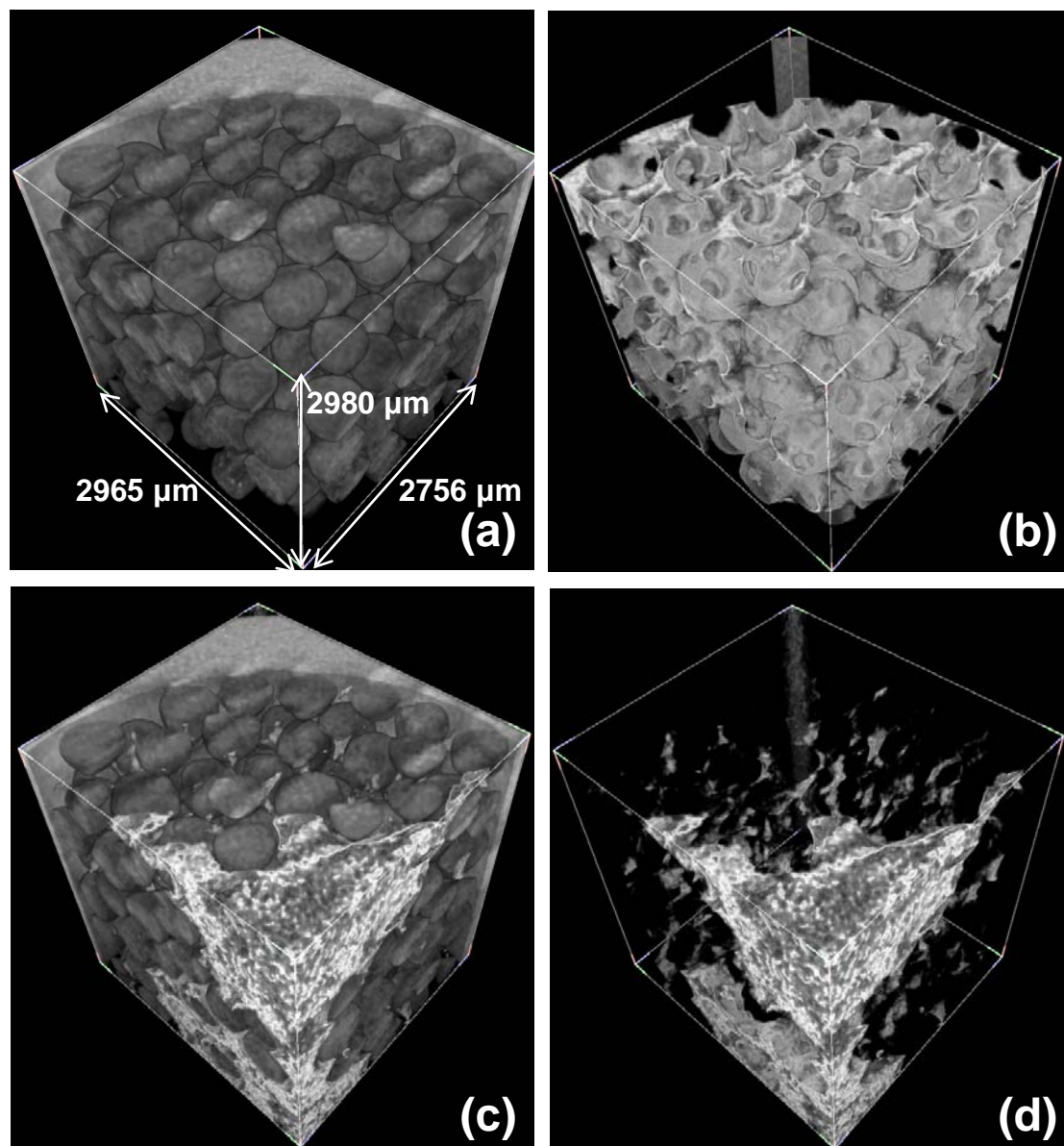
Figure 12. 3-D images of methane hydrate in host glass beads after 15:15 h of cooling. The images were reconstructed from 400 slices such as those shown in Fig. 11. An embedded 2-D histogram tool in Drishti and a transfer function for each phase were used to differentiate (a) Aluminum cell and glass beads, (b) 5wt% aqueous solution, (c) methane hydrates within glass beads, and (d) only methane hydrates from same volume.